Title: **Tbx3 is required for mammalian retinal angiogenesis.**

Running title: TBX3 required for retina angiogenesis

Derbyshire, M.*[1,2], Akula, S.*[1,2], Wong, A.[1,2], Rawlins, K.[1], Voura, E.[1], Brunken, W.J.[1], Zuber, M.E.[1], Moon, A.M.[3,4,5], and Viczian A.S[1†].

*these authors contributed equally to this work
†corresponding author

1, Ophthalmology and Visual Sciences Department, Upstate Medical University, 750 East Adams Street, Syracuse, NY 13210.
2, College of Medicine, Upstate Medical University, 750 East Adams Street, Syracuse, NY 13210.
3, Department of Molecular and Functional Genomics, Weis Center for Research, Geisinger Clinic, Danville, PA 17822.
4, Department of Human Genetics, University of Utah, Salt Lake City UT 84112
5, The Mindich Child Health and Development Institute, Hess Center for Science and Medicine at Mount Sinai, New York, NY, USA 10029

Keywords: retina, angiogenesis, hypovascular, Tbx3, retinal ganglion cell, ipRGC, astrocyte, melanopsin, FEVR, ROP.

Summary Statement

TBX3 is a multifunctional protein important for frog eye development. This is the first study showing that TBX3 is critical for mammalian eye formation, controlling the function of key cells required for angiogenesis.

Abstract

Neural tissue formation requires coordinated, interwoven development of both neural and vascular cells. Spatially distinct regions of the central nervous system (CNS) express factors that are predicted to affect vasculature in one area but not another, yet an example of this idea has not been found. Due to its accessibility, the eye is an excellent tissue to study this question. The factor TBX3 is required for frog eye development, yet its role in mammalian eye formation was not known. To determine how *Tbx3* loss-of-function affected eye formation, we crossed the validated *Tbx3*-floxed mice with the optic cup-Cre recombinase driver, *BAC-Dkk3-CRE*. We confirmed earlier expression studies of *Tbx3* RNA and protein in the embryonic dorsal optic vesicle and, postnatally, in sporadic clusters of cells of the inner nuclear layer. Surprisingly, we also found TBX3 in astrocyte precursors at P0. With *Tbx3* loss, blood vessels were malformed throughout the retina, but with more severe effects seen in the dorsal retina. Astrocyte precursors were reduced in number and failed to form a lattice at the dorsal edge. We next examined retinal ganglion cells, as they have been shown to play a critical role in retinal angiogenesis. We found that a subset of intrinsically photosensitive retinal ganglion cells (ipRGCs) were missing melanopsin in the dorsal half of the retina. In previous studies, loss of melanopsin has been linked to hyaloid artery persistence, which we also observed in the *Tbx3* cKO retina. Together, these results show that TBX3 is required for retinal angiogenesis.

Introduction

As with the rest of the central nervous system, retinal development requires the synchronized formation of neural and vascular tissue for visual function. Vasculature development in the eye begins with the formation of the hyaloid artery in the embryo, which nourishes the optic cup. During development, the early mouse retina remains avascular until differentiation of retinal cells causes an increase in metabolic demand. The differentiated cells release proteins that stimulate the migration and proliferation of astrocytes from the optic nerve just prior to birth (reviewed in (Tao and Zhang, 2014; Selvam et al., 2018; Sun and Smith,

2018)). Astrocyte precursors cling onto the axons of retinal ganglion cells as they migrate into the retina (O'Sullivan et al., 2017; Paisley and Kay, 2021). Migrating astrocyte precursors then produce signals to attract endothelial cells into the retina, which in turn, produces proteins that cause the astrocytes to differentiate. Therefore, coordinated activity of neural, astrocytes and endothelial cells are essential for nascent blood vessels to begin forming a steady blood supply to the retina. Factors were identified that affect angiogenesis in the CNS, but not in non-CNS tissue (Daneman et al., 2009). These factors were found in spatially restricted area, and it was predicted that angiogenesis would form differently in different regions (Daneman et al., 2009), yet, to our knowledge, this has not been found. Disruption of signals from either the vascular cells or neurons halts angiogenesis throughout the retina, creating a hypovascular retina seen in Retinopathy of Prematurity (ROP) and Familial Exudative Retinopathy (FEVR) (Selvam et al., 2018). Mutations in Wnt signaling pathway components, like the Wnt receptor Frizzled4, are linked to these syndromes (Rao et al., 2017; Tang et al., 2017; Li et al., 2018; Tauqeer and Yonekawa, 2018), and are responsible for 50% of FEVR cases (Selvam et al., 2018). The genetic mutations causing the remaining half of the FEVR patients are unknown (Selvam et al., 2018).

The signals, which drive creation of the retinal vasculature, function in concert with other signals that cause regression of the hyaloid artery. The hyaloid artery is a transient fetal vascular structure in many vertebrates. Its regression is triggered by signals from intrinsically photosensitive retinal ganglion cells (ipRGCs) (Rao et al., 2013; Nguyen et al., 2019). Failure of the hyaloid vessels to regress leads to persistent fetal vasculature (PFV), which leads to intraocular hemorrhage and impairment of vision. Despite decades of study, and the importance to human disease, a complete understanding the molecular regulation of retinal vascular development is still lacking.

In this study, we have identified a key factor, *Tbx3*, in cell types affecting retinal vascular development. In the frog, *Xenopus laevis*, *tbx3* is expressed in the eye field prior to optic vesicle formation where it plays an essential role early in eye formation (Takabatake et al., 2000; Wong et al., 2002; Zuber et al., 2003; Weidgang et al., 2013; Motahari et al., 2016). Later in ocular development, *Tbx3* is found in the dorsal half of the optic cup in both frog and mouse (Chapman et al., 1996; Takabatake et al., 2000; Sowden et al., 2001; Wong et al., 2002; Weidgang et al., 2013). Functional studies of the role of *Tbx3* in mammalian eye formation have not been done. An initial gene deletion of murine *Tbx3* did not study the eye (Davenport et al., 2003) and produced only a hypomorphic deletion (Frank et al., 2013). Thus, a conditional ablation strategy

was developed (Frank et al., 2012; Frank et al., 2013) and used successfully to study the role of *Tbx3* in several other tissues (Kumar P et al., 2014; Emechebe et al., 2016; Lüdtke et al., 2016; Aydoğdu et al., 2018; Quarta et al., 2019; Kaiser et al., 2021).

In this study, we investigated the role of *Tbx3* in mammalian retinal development for the first time using a combination of expression studies and reverse genetics to probe function. To our surprise, we found that *Tbx3* is expressed not only in embryonic retinal progenitors, but also in retinal astrocyte precursors at P0. To investigate the effect of *Tbx3* loss-of-function on retinal development, we crossed mice bearing the *Tbx3* conditional allele (Frank et al., 2013) with an eye-specific Cre driver (BAC-Dkk3-Cre). In the *Tbx3* conditional knockout mice, we observed that the hyaloid artery persisted, and the retina was hypovascular. We found fewer astrocytes in the *Tbx3* conditional knockout retina at P9, and by P30, the astrocytic lattice was malformed in the dorsal retina. With *Tbx3* loss, we also found thinner optic nerves and fewer intrinsically photosensitive retinal ganglion cells. Together, these results suggest that TBX3 is required for mammalian eye formation and that this conditional knockout could potentially be a new mouse model for hypovascular diseases. It also the first example of the hypothesis that angiogenesis is affected by spatially distinct cues.

Results

To determine the expression pattern of *Tbx3* in the embryonic eye, a tamoxifen-inducible Cre was knocked into the *Tbx3* gene locus ($Tbx3^{mcm/+}$) (Emechebe et al., 2016)). These animals were then crossed with the $Rosa^{LacZ}$ reporter line ($Tbx3^{mcm/+}; Rosa^{LacZ/+}$; Fig. 1A, B). Consistent with earlier studies, *LacZ* was expressed at E10.5 and E11.5 in the dorsotemporal region of the optic cup with gradual reduction in the ventral eye (Chapman et al., 1996; Behesti et al., 2006). *In situ* hybridization to detect *Tbx3* mRNA showed a similar gradient of transcript expression: high in the dorsal to low in the ventral neural retina (Fig. 1C,D). Expression was not detected in the presumptive retinal pigment epithelium (pRPE; Fig. 1C). In newborn mice, we find that *Tbx3* mRNA is confined to the base of the neuroblast layer (arrows, Fig. 1E-E'') and in cells at the inner limiting membrane (arrowhead, Fig. 1E'). To better visualize TBX3 expression, we used the recombined $Tbx3^{GFP}$ conditional reporter allele $Tbx3^{GR/+}$, in which GFP has been knocked into the endogenous *Tbx3* gene (TBX3-GFP). We used antibody immunostaining for GFP protein to enhance detection, as previously described (Frank et al., 2012). Relatively little GFP staining was detected in wild-type sibling embryos (Fig. 1F), while in $Tbx3^{GR/+}$ embryos, we

detected embryonic TBX3-GFP in the same gradient pattern with a few GFP-positive cells at the optic nerve head (arrows, Fig. 1G'). At E13.5, Pax2 is expressed in the optic nerve head in cells fated toward an astroglial lineage (Soukkarieh et al., 2007; Tao and Zhang, 2014; Bosze et al., 2021). Co-immunostaining with the anti-Pax2 and GFP antibodies, we detected GFP at low levels in some Pax2-positive cells (arrows, Fig. 1G'-G''' and Fig. S1A-B''). Pearson's correlation co-efficient for GFP/Pax2-positive cells in the retina averaged 0.337 ± 0.05 (>4 sections measured per eye; N=2), indicating low correlation. At birth, Pax2 marks astrocyte precursors as they migrate into the retina (Mi and Barres, 1999; Chu et al., 2001). We flat mounted retinas at P0, immunostained with anti-Pax2 and GFP antibodies, and imaged whole retinas using both the confocal and stereomicroscopes (Fig. S1 C,D and Fig. 1H,I). Flat mounts of P0 retinas from sibling WT have no visible GFP expression, yet TBX3-GFP mice show co-labeling with GFP and Pax2 (Fig. 1H,I and Movies 1,2). Together, these data suggest that *Tbx3* is initially expressed in retinal progenitors, and possibly some Pax2-positive glial progenitors while later, it is expressed in astrocyte precursors, as well as cells in the neuroblast layer.

To investigate the effects of *Tbx3* loss on early eye formation, we selected the *BAC-Dkk3-CRE* mouse line (Sato et al., 2007). To confirm its specificity, *BAC-Dkk3-CRE* mice were crossed with the Ai9 reporter line, which expresses tdTomato in the presence of CRE protein activity. As previously reported, we found weak but detectable expression of the tdTomato reporter in a few retinal progenitors of the E9.5 optic vesicle (Fig. 1J). By E11.5, tdTomato was detected throughout the neural retina, optic stalk and in the lens epithelium (Fig. 1K). Western blot analysis confirmed the loss of TBX3 protein in the *BAC-Dkk3-CRE;Tbx3*$^{\Delta Fl/\Delta Fl}$ retina (Fig. 1L). Preliminary observations indicated abnormal blood vessel formation in the eyes of *BAC-Dkk3-CRE;Tbx3*$^{\Delta Fl/\Delta Fl}$ mice. Therefore, we investigated the effect of *Tbx3* loss on retinal vasculature development.

Retinal vasculature develops postnatally in mice and blood vessels reach the edge of the retina by P9 (Dorrell et al., 2002; Stalmans et al., 2002). Therefore, to determine the effect of *Tbx3* loss on angiogenesis, we stained P9 retinal flat mounts using isolectin B4 (IB4) to visualize vascular endothelial cells (Fig. 2A,A'). *BAC-Dkk3-CRE;Tbx3*$^{\Delta Fl/\Delta Fl}$ mice (*Tbx3* cKO) had severe disruption of vasculature development, in that the blood vessels failed to advance to the edges of the retina (Fig. 2B,B'). The hyaloid artery (HA) provides blood to the developing embryonic eye. Postnatally the HA regresses and is substantially reduced by P8 (Rao et al., 2013). While we observed remnants of this structure in some wild-type samples (arrow, Fig. 2A'), the vessel were easily observed in *Tbx3* cKO retinas (Fig. 2B,B'). We then measured the

dorsal and ventral retinal surface areas covered by the vasculature (Fig. 2C). There was a decrease in the ventral vascular coverage in comparing *Tbx3* cKO and wild-type siblings (71 ± 5.9%). However, the retinal vasculature of the dorsal *Tbx3* cKO retina exhibited more loss, measuring one quarter of the surface area occupied by wild-type siblings (Fig.2C; 24.9 ± 3.0%). These results indicate a requirement for *Tbx3* in the normal development or maintenance of the early postnatal retina vasculature. It is also possible that *Tbx3* loss simply causes a delay in forming the retinal vasculature, so we next looked at blood vessels after they matured.

The retinal vascular plexus grows into a tri-layered structure composed of superficial, intermediate, and deep layers. Plexus formation is complete at approximately three weeks of age (Selvam et al., 2018). Retinas were collected from P26 mice to determine the effect of *Tbx3* loss on the mature vascular plexus. Flat mounts were prepared and stained to detect vascular endothelial cells. In contrast to the wild-type structure (Fig. 3A-C), the vascular plexus of *Tbx3* cKO retinas was abnormal (Fig. 3D-F). Confocal optical sections showed the superficial layer did not extend to the periphery of the dorsotemporal retina in *Tbx3* cKO mice (Fig. 3D,F, dashed red line marks areas; Movie 3). In addition, the dorsal vein was thinner and missing from the edge of conditional knockout retinas (red arrowheads, Fig. 3G vs. 3H; Movie 3). The *Tbx3* cKO vascular plexus also appeared less complex when compared to wild-type siblings (Fig. 3G,H). To further define the apparent reduction in complexity, we measured both the vasculature's branch point and length density in *Tbx3* cKO and wild-type animals (Fig. 3I; quantitation shown in Fig. S2). We found a reduction in both branch point density (WT, 1537 ± 99; cKO, 1034 ± 106 junctions/mm^2) and vascular length density (WT, 6.48 ± 0.12; cKO, 5.20 ± 0.26 mm/mm^2) in mutants (Fig. 3I). Confocal imaging of central retinal sections from controls showed the normal tri-layered vasculature and inter-plexus branching (Fig. 3J and Movie 4). In contrast, *Tbx3* cKO retinas lacked the superficial plexus (Fig. 3K and Movie 5). Cryostat sections show vessels in all three layers in the wild-type (Fig. 3L and Fig. S3A), while in the absence of *Tbx3*, some regions (as in dashed regions shown in Fig. 3F) were missing both the superficial and deep layers (Fig. 3M and Fig. S3B). Glial fibrillary acidic protein (GFAP) labels Müller glia and astrocytes at this age. We detected less dense GFAP staining in the *Tbx3* cKO retina and that the outer nuclear layer is thinner at the dorsal edge in the mutants (bracket, Fig. 3M). Less GFAP staining suggests fewer astrocytes in the *Tbx3* cKO retina. Together, these results indicate that the formation of a normal adult retinal vasculature requires *Tbx3*.

Endothelial cells enter the retina perinatally, following astrocytes that form a lattice ahead of the endothelial cells (Fig. 4A,A'). If the reduction in angiogenesis in the *Tbx3* cKO

begins at this early time point, then we would expect the lattice to be disrupted in mutant mice. Flat mounts at P2 showed reduced endothelial cells and astrocytes in the *Tbx3* cKO retina (Fig. 4B,B'). Retinal astrocyte precursors express the paired-box transcription factor, Pax2, and the growth factor receptor, PDGFRα, but not glial fibrillary acidic protein (GFAP). As they mature, astrocytes express both Pax2 and GFAP (Mi and Barres, 1999; Chu et al., 2001). We found stunted migration and statistically fewer Pax2-positive astrocyte precursors in the retina at P2 in both the dorsal and ventral retinas (Fig. 4C-F). As we found TBX3 expressed in early astrocyte precursors (Fig. 1I), the stunted growth or migration of astrocyte precursors suggests that TBX3 may be required by these cells as they move into the retina. We further reasoned that lattice formation may recover if TBX3 is only required at this initial stage, and therefore, next looked at older animals.

By P9, astrocytes reached the edge of the wild-type retina (Fig. 5A) yet failed to do so in the conditional knockout (Fig. 5B). Even at one month of age, astrocytes failed to reach the dorsal edge of the cKO retinas (compare Fig. 5C to 5D,D'). We compared the surface area occupied by astrocytes at P9 and P30, normalized to the average wild-type retinal surface area. We observed a statistically significant difference between wild-type and *Tbx3* cKO retinas at P9 and P30 (P9 WT, 1.0 ± 0.01; P9 cKO, 0.58 ±0.02; P30 WT, 0.97±0.01; P30 cKO, 0.76 ±0.03; Fig. 5E). We also observed significant growth between P9 and P30 ($p<0.001$), indicating that signals promoting astrocyte lattice formation persist in the absence of TBX3 (Fig. 5E). These results indicate that astrocytes require TBX3 to form the astrocytic lattice required for normal retinal vasculature formation. Astrocyte lattice formation can also be disrupted with the loss of retinal ganglion cells, as in the *Atoh7* knockout retina. Retinal ganglion cells of these mice are reduced by 95% and grow a severely stunted astrocytic lattice (Edwards et al., 2012; O'Sullivan et al., 2017). Thus, it is possible that TBX3 is indirectly affecting astrocytes by functioning within ganglion cells. Previous studies have also shown that hyaloid artery regression is dependent on signals from intrinsically photosensitive retinal ganglion cells (Rao et al., 2013; Nguyen et al., 2019). We observed that the hyaloid artery persisted in the mutant retina (Figs. 2B,B' and 5B). Therefore, we next investigated whether retinal ganglion cell formation requires TBX3.

We found that optic nerves were significantly thinner in cKO mice compared to their WT littermates (Fig. 6A-C), measuring 71 ± 3.9% of the average WT optic nerve (Fig. 6D). This suggests that fewer retinal ganglion cells may be present in the cKO retina. After sectioning and staining P9 retinas using the anti-Islet1/2 antibody, we observed a significant decrease in dorsal Islet1/2-positive retinal ganglion cells (RGCs) in the cKO retina, but no difference in the ventral

region (dorsal WT: 37.7 ± 2.8 cells; dorsal cKO: 27.7 ± 2.4 cells; Fig. 6E-G). This suggests that *Tbx3* is required by a subset of Islet1/2-expressing dorsal RGCs. Islet1 is thought to regulate the formation of most RGCs, including melanopsin-expressing (OPN4) intrinsically-photosensitive ganglion cells (ipRGCs) (Mao et al., 2014). We stained flat mounts with the anti-OPN4 antibody and measured the density of OPN4-positive cells for each sample, normalized to the average wild-type control. When blood vessels were stunted at P9, we observed significant reduction of ipRGC density in the dorsal (WT: 1.00 ± 0.11; cKO: 0.57 ± 0.06) and nasal/temporal petals (WT: 0.83 ± 0.07; cKO: 0.46 ± 0.06), but not in the ventral petals (Fig. 6H-J). Overall, we found significantly less ipRGCs in cKO retinas at P9 (WT: 1.00 ± 0.10; cKO: 0.63 ± 0.09). This difference persists when measured at P30 (WT: 1.00 ± 0.09; cKO: 0.68 ± 0.02), suggesting that the reduction in ipRGCs was not due to a delay of differentiation (Fig. 6K-L). Together, these results indicate that TBX3 is required for a subset of OPN4-expressing ipRGCs in the dorsal half of the retina, which control vascular formation in this region.

Discussion

Our results provide the first evidence that TBX3 is required for mammalian eye formation. We have found that *Tbx3* mRNA and protein is expressed in embryonic retinal progenitors and postnatal astrocyte precursor cells. When we remove *Tbx3* from the embryonic optic cup, the hyaloid artery persists in P9 mice and retinal vascular formation is stunted. At P9, the vascular defect is found throughout the retina, but more severe in the dorsal region. The dorsal vascular plexus continues to be affected by *Tbx3* loss in the older animals, including the loss of the superficial layer of the vascular plexus and the astrocyte lattice. We observe that in the absence of *Tbx3,* fewer astrocyte precursors are present in the retina. As the retina matures, astrocyte lattice formation recovers in all but the dorsal region. Localization of the defect to the dorsal retina is the first report of a spatially distinct defect in angiogenesis, which was predicted over a decade earlier, but not shown (Daneman et al., 2009). In this area, we find fewer Islet1/2-positive and intrinsically photosensitive retinal ganglion cells. One interpretation is that these cells fail to attract or stimulate the proliferation and/or migration of astrocyte precursors that form the dorsal lattice. In contrast, our data could also suggests that TBX3 may function within astrocytes, controlling their development and loss of *Tbx3* in ipRGCs simply affects hyaloid artery persistence at P9 in the *Tbx3* cKO retina. The fact that we are observing abnormal vascular plexus and astrocyte formation in the dorsal retina, supports the hypothesis

that the dorsal retinal ganglion cells lost are the underlying defect. In any case, these results provide a fruitful new model to study retinal hypovascularization.

Patients with syndromes, including Norrie disease (ND) or Familial Exudative Vitreoretinopathy (FEVR), develop hypovascular retinas that lead to congenital blindness (Wang et al., 2020). These diseases have been associated with mutations in Wnt/Norrie signaling pathway ligands (*LRP5*, *NDP*), receptor (FZ4) and a co-receptor (*TSPAN12*), as well as a kinesin family member 11 (*KIF11*) (Rao et al., 2017; Tang et al., 2017; Li et al., 2018; Tauqeer and Yonekawa, 2018). Mutations found in these proteins have been studied using mouse models of these mutant alleles (Luhmann et al., 2005; Junge et al., 2009; Ye et al., 2009; Ye et al., 2010; Collin et al., 2013; Wang et al., 2020). Canonical Wnt signaling occurs when Wnt ligands bind to their receptors, which leads to stabilizing β-catenin that can regulate target downstream genes. While most of these factors work in the canonical Wnt/Norrie signaling pathway, *KIF11* has been shown to function independently from β-catenin signaling in retinal angiogenesis (Wang et al., 2020). In separate studies, TBX3 has been shown to work in Wnt signaling and with a kinesin protein. In pull-down assays, TBX3 has direct interaction with another kinesin family member, KIF7, and affects its function (Emechebe et al., 2016). In vivo, TBX3 has been shown to work with, or downstream of, the Wnt signaling pathway in ureter, lung and human colorectal cancer (Lüdtke et al., 2016; Aydoğdu et al., 2018; Zimmerli et al., 2020). In future studies, we plan to determine in which molecular pathway Tbx3 functions.

Another characteristic, besides hypovascularization, shared among some FEVR patients is a persistent hyaloid artery (Pendergast et al., 1998; Dhingra et al., 2006; Wu et al., 2007; Robitaille et al., 2009; Payabvash et al., 2015). In mice, this defect has also been found with the loss of melanopsin (*OPN4*), however, in these mutant mice, the retina is hypervascular, rather than hypovascular (Rao et al., 2013). In contrast, the *Tbx3* cKO has a persistent hyaloid artery as well as a hypovascular retina. Along with FEVR, these phenotypes are also present in a mouse model of Retinopathy of Prematurity, in which neonatal pups are exposed to elevated oxygen levels from P0 to P4 (Perelli et al., 2021). In these mice, angiogenesis is globally affected, where only about 25% of the entire retinal surface was covered by P8 (Perelli et al., 2021). In comparison, vessels covered approximately 25% of the dorsal *Tbx3* cKO retina. Therefore, it is possible that Tbx3 is required for the hypoxia signaling pathway either in neurons or in astrocytes. Moreover, the similarities between the phenotypic changes we observe in the conditional *Tbx3* knockout mouse and those in FEVR/ROP patients suggests the exciting possibility that the *Tbx3* cKO may serve as a new mouse model for these human diseases.

We discovered that TBX3-GFP is expressed in astrocyte precursors. We found that *Tbx3* loss causes a reduction in astrocyte precursors in the newborn retina. Astrocytes arise from the optic disc progenitor zone which surrounds the optic nerve disc (Mi and Barres, 1999; Mi et al., 2001). During migration into the retina, they proliferate prior to contact with endothelial cells, since the endothelial cells cause their differentiation (Mi et al., 2001). Our results could be explained by either a reduction in astrocyte precursor proliferation or reduced migration due to corrupt cues from the neural retina lacking *Tbx3*. Retinal ganglion cells release platelet-derived growth factor A-chain (PDGF-A), which attracts astrocytes, but PDGF-A also causes proliferation of these cells (Fruttiger et al., 1996). As we have also observed a loss of RGCs in the dorsal retina, it is possible that loss of *Tbx3* indirectly affects astrocyte proliferation/migration. It is also possible that in astrocyte precursors TBX3 contributes to the regulation of a gene that controls astrocyte proliferation - like the transcription factor Tailless (*Tlx*) (Miyawaki et al., 2004; Uemura et al., 2006). We previously found that misexpression of frog *tbx3* (also known as ET for 'Eye T-box') induced *tll* expression (Zuber et al., 2003). It will be important to investigate the role of TBX3 in regulating *Tlx* expression and astrocyte proliferation and/or migration.

Later, in the differentiated retina we found truncation of the astrocytic lattice in the dorsal-temporal region. Blood vessels were growing into the area, but they failed to form a superficial plexus. Endothelial cells build the superficial plexus in response to the chemical and structural cues of the underlying astrocytes (Jiang et al., 1994; Jiang et al., 1995; Stone et al., 1995; Zhang and Stone, 1997; Fruttiger, 2007). Therefore, it is logical that loss of dorsal astrocytes due to loss of *Tbx3* would lead to superficial plexus loss in that region. Finding dorsal intermediate blood vessels in the absence of the superficial and sometimes deep layers is curious. The deep plexus formation has been linked to spontaneous activity from cholinergic starburst amacrine cells (Weiner et al., 2019). Meanwhile, formation of the superficial and deep, but not intermediate, plexus layers requires the activity of the hypoxic response pathway (via the von Hippel-Lindau factor (Vhl) found in amacrine and horizontal cells (Usui et al., 2015). In a recent study that used single cell PCR to generate a genetic regulatory network in the mouse retina, *Tbx3* was found in amacrine and Müller glia (Lyu et al., 2021). Overexpression of TBX3 in retinal progenitors at P0 led to an increase of amacrine, retinal ganglion cells, Müller glia, and bipolar cells, but repressed formation of rod photoreceptors (Lyu et al., 2021). Therefore, in future studies, we will determine the effect of *Tbx3* loss on all types of retinal neurons.

Materials and methods

Mice

Generation of transgenic mouse strains, BAC-Dickkopf3:cre (*BAC-Dkk3-Cre*)(Sato et al., 2007), *Tbx3*^{mcm} (Emechebe et al., 2016), *Tbx3*-floxed and *Tbx3*^{G}, (Frank et al., 2012; Frank et al., 2013) were previously described and maintained on a C57Bl/6J background. Tamoxifen treatment was done as previously described (Park et al., 2008). The Ai9 Cre reporter line (B6.Cg-*Gt(ROSA)26Sor*$^{tm9(CAG\text{-}tdTomato)Hze}$/J) was obtained (The Jackson Laboratory, stock#: 007909). We backcrossed the *Tbx3*-floxed line to five generations into a C57Bl/6J background. We used sibling conditional knockout (*BAC-Dkk3-Cre*$^{+}$;*Tbx3*$^{\Delta Fl/\Delta Fl}$) and wild-type (*BAC-Dkk3-Cre*-negative;*Tbx3*$^{Fl/+}$), as controls. At least two litters were used for analysis with the number of mice (N) indicated in each figure. We observed no difference in levels of TBX3 protein in male and female samples by western blot (Fig. 1L). When possible, we divided samples into male/female sample sets and found no statistical differences. Therefore, we performed our analysis on a random mixture of both male and female mice. Animals were euthanized according to established guidelines set forth by the American Veterinary Medical Association. This study was approved by Upstate's Institutional Animal Care and Use Committee.

Genotyping

Ear punches or tail snips (1-2 mm) were incubated overnight at 55˚C in 100 μl lysis buffer (10mM Tris, pH 8.0, 100mM NaCl, 10mM EDTA, pH 8.0, 0.05% SDS) and 80 μg Proteinase K (Sigma; catalog #: P2308; 20 mg/ml stock; powder dissolved in 10 mM Tris HCl, pH 7.5, 20 mM calcium chloride, and 50% glycerol). Samples were vortexed, in the morning, and place back at 55˚C for 30-60 minutes. Samples were spun down at 14,000g for 15 minutes and then 70μl of supernatant was carefully drawn off and placed in 200μl ice cold isopropanol. The mixture was inverted several times, then spun at 4˚C, 14,000g for 10 minutes. Supernatant was poured off and the pellet was washed twice with 70% ethanol, dried and resuspended in 10 mM Tris, pH 8.0. PCR was performed as described in Table S1 with 0.25 units EconoTaq enzyme (Biosearch Technologies), 1X EconoTaq Buffer, 200μM dNTPs, 0.25μM primers for all reactions, except *Tbx3*^{GR} reactions that included 2% DMSO.

Immunostaining

For sections, isolated eyes with a pierced cornea were submerged in 4% paraformaldehyde/1X PBS for either 30 min on ice (for *in situ* hybridization or GFP immunostaining) or overnight (for all other immunostaining). The tissue was washed three times for 5 minutes in 1X PBS. Then, it

was incubated with increasing concentrations of sucrose (5%, 10%, and 20%) and changed out when the eye sunk to the bottom of tube in each solution. The eyes were then mounted in O.C.T. (Tissue-Tek), frozen on dry ice and cryostat sectioned at 20μm and the slides stored at -20˚C until immunostained. We immunostained sections by using standard conditions. Briefly, frozen slides were heated at 37˚C for 10 minutes, washed at room temperature (RT) in 1XPBS for 5 minutes, incubated at RT in blocking solution (Table S2) for an hour and then incubated at 4˚C with primary antibody (Table S2) in primary antibody solution [1X PBS/1% bovine serum albumin (Sigma Aldrich)/0.3% Triton X-100 (Sigma Aldrich)] overnight. The next day, we washed slides 3 times for 5 minutes in 1X PBS/0.1% Triton X-100 (1X PBST) and then added the corresponding secondary antibody (Table S2) in 1X PBST with DAPI (10μg/ml) for an hour at RT. Slides were washed 3 times in 1X PBST and coversliped with FluorSave (MilliporeSigma) and 2% DABCO (1,4-Diazabicyclo[2.2.2]octane; Sigma). Flat mounts were stained with isolectin B4 (IB4) and immunostained with antibodies, as described in Gnanaguru et al., 2013. Briefly, retinas were separated from RPE and incisions were made to flatten the tissue. Retinas were placed onto a round coverslip, liquid gently siphoned off and stiffened with a drop of 100% methanol, then submerged in methanol for at least 30 minutes. Flat mounts were either stored at -20˚C or rehydrated through a series of washes with increasing amounts of 1X PBS (75%, 50%, 25%, 0% methanol in 1XPBS). The retinas were washed once in 1X PBST, then transferred to a 1.7ml tube in 1X PBST and replaced with 100μl blocking solution with 0.1% NaAzide (VWR). The tissue was incubated at 4˚C overnight. At least 24 hours later, the blocking solution was replaced with antibodies or IB4 in primary antibody solution with 0.1% NaAzide and left at 4˚C for 2-3 days. Retinas were washed with 1X PBST 3 times for 2 hours at RT and then left overnight in a fourth wash. Secondary antibody in 1X PBST (Table S2) was added for 2 hours at room temperature. Tissue was washed 3 times for 20 minutes each in 1X PBST. Reinforcement labels (Avery 5722) were pasted onto slides and retinas were placed inside each ring with mounting solution [FluorSave (MilliporeSigma) and 2% DABCO (1,4-Diazabicyclo[2.2.2]octane; Sigma)] and a round cover slip added on top.

RNA in situ hybridization

RNA was extracted from mouse retinas using RNAzol RT and cDNA was generated using GOSCRIPT reverse transcriptase according to the manufacture's protocol. *Tbx3* cDNA was PCR amplified with Herculase II using the following primers: BamH1 mTbx3 Forward (5' aatggatccaCCATGAGCCTCTCCATGAG 3') and Xho1 mTbx3 Reverse (5'

aattctcgagTTAAGGGGACCCGCTG 3') according to the manufacture's protocol. The PCR product was cut with BamH1 and Xho1 and cloned directly into pCS2R cut with the same enzymes. DIG-labeled sense and antisense cRNA probes were manufactured from linear DNA made using these same two restriction enzymes. In situ hybridization was done as previously described (Viczian et al., 2003; Martinez-De Luna et al., 2013).

Microscopy

Images were taken using a Leica DM600B stereomicroscope outfitted with a MicroPublisher 6 camera (Teledyne Q-Imaging), and, where applicable, stitched together using the Volocity (v6.3) software. Confocal images were taken with the Zeiss LSM780 confocal and Zeiss Imaging Software. Images of WT and cKO samples were equally processed for brightness and contrast in Adobe Photoshop 2022. Cell counts and analysis were performed under double-blind conditions. Sample types were revealed when entering numbers into the statistics software (Prism v9.3.1).

Measurement of vasculature

We measured the surface area occupied by retinal structures (either endothelial or astrocyte markers) and the volume of the whole surface area using Volocity software. The ratio of retinal structure to whole retinal surface was calculated and statistically analyzed. The migration of Pax2+ cells was measured within 500μm of the dorsal petal (counting 10 cells per sample). The area occupied by Pax2+ cells was measured by adjusting the threshold in ImageJ and comparing that to the area of the dorsal retina.

Western immunoblotting

Protein was extracted from both retinas of sibling newborns and processed for western blot analysis, as previously described (Wong et al., 2015). Anti-TBX3 antibody (1:2000; Bethyl Lab, Inc.) in 5% milk, 0.1% Tween/1XTBS was used.

Statical analysis

Prism (v9.3) was used for statistical analysis. Measurements were done blind to the genotype of the sample. We normalized data by taking the average wild-type measurement in each litter and dividing it into each sample in that litter. Cell density is the measure of cells per unit area. Graphs and data are reported as mean ± the standard error of the mean (s.e.m.). Each point on a graph is the average of two eyes from a single animal (N).

Acknowledgments

We would like to thank Jason Shandler, Amanda Bielecki, Abigail Snow, Stephen Sanabria and Dominica Colavito for their excellent assistance in genotyping animals and performing cell counts. We would also like to thank Dr. Arvydas Matiukas for his assistance in using the confocal microscope in Neuroscience Microscopy Core. The anti-Islet1/2 antibody was obtained from the Developmental Studies Hybridoma Bank, created by the NICHD of the NIH and maintained at The University of Iowa, Department of Biology, Iowa City, IA 52242.

Competing interests

The authors declare no financial nor competing interests.

Funding

This study was supported by the National Institutes of Health (R21 EY029114 to A.S.V; R01 EY012676 to W.J.B; R21 EY030654 to M.E.Z), and grants to the Ophthalmology and Visual Sciences Department from Research to Prevent Blindness (Unrestricted Award) and the District 20-Y Lions Club.

Figure Legends

See figures and tables.

Figure 1

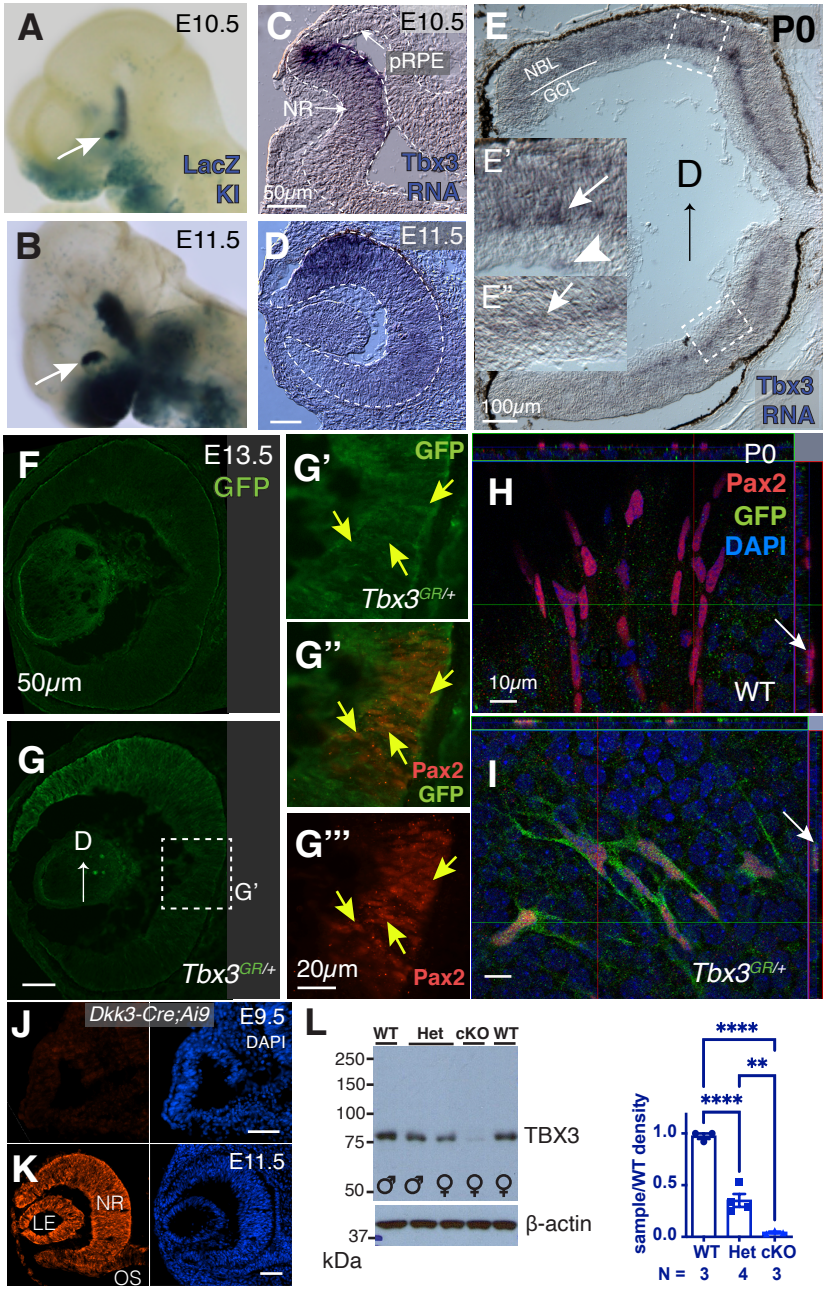

Figure 1. TBX3 expression in the neural retina and efficient conditional knock-out (cKO) using the BAC-DKK3-Cre driver.

A,B) LacZ activity under the control of the endogenousTbx3-locus (LacZ KI: Tbx3mcm). Arrow points to the dorsotemporal region of the eye at embryonic days 10.5 (E10.5) and 11.5 (E11.5).

(C-D') In situ hybridization using Tbx3 antisense RNA at E10.5 and E11.5. Outline of developing eye in C,D; pRPE, presumptive RPE; NR, neural retina.

(E) Tbx3 mRNA expression in newborn retina.

(E',E") Inlays of dorsal and ventral retinas. Arrows point to cells at the base of the neuroblast layer and arrowhead to cells at inner limiting membrane.

(F) Wild-type sibling of transgenic embryo (G) expressing GFP under the control of the endogenous Tbx3-locus (*Tbx3*$^{GR/+}$) immunostained with anti-GFP antibody (green) at E13.5. Dashed box shows region magnified. (G'-G''') Close-up of boxed region in G immunostained with an anti-Pax2 (red) and GFP antibodies (see Fig. S1 for more images).

(H) Confocal flat mount image of newborn retina from sibling wild-type and (I) *Tbx3*$^{GR/+}$ mice immunostained with anti-Pax2 and GFP antibodies. Orthogonal view on top and side. Arrow points to cell that is positive for Pax2 in H and positive to Pax2 and GFP in I.

(J,K) *BAC-Dkk3-CRE* expression pattern is detected using Ai9 reporter line expressing tdTomato. Cre activity is first detectable in the neural retina at E9.5 and is expressed throughout the neural retina (NR), lens epithelium (LE) and optic stalk (OS) by E11.5.

(L) Western blot of P0 retinas collected from wild-type (WT, *Tbx3*$^{Fl/+}$), heterozygous (Het, *BAC-Dkk3-CRE;Tbx3*$^{\Delta Fl/+}$), and homozygous knockout (cKO, *BAC-Dkk3-CRE;Tbx3*$^{\Delta Fl/\Delta Fl}$) siblings. Graph shows mean ± s.e.m. of 2 litters. No statistical differences in Tbx3 expression were observed in males and females. Ordinary one-way ANOVA test with multiple comparisons was used to determine statistical significance. ****, p=0.00005; **, p≤ 0.01.

Figure 2

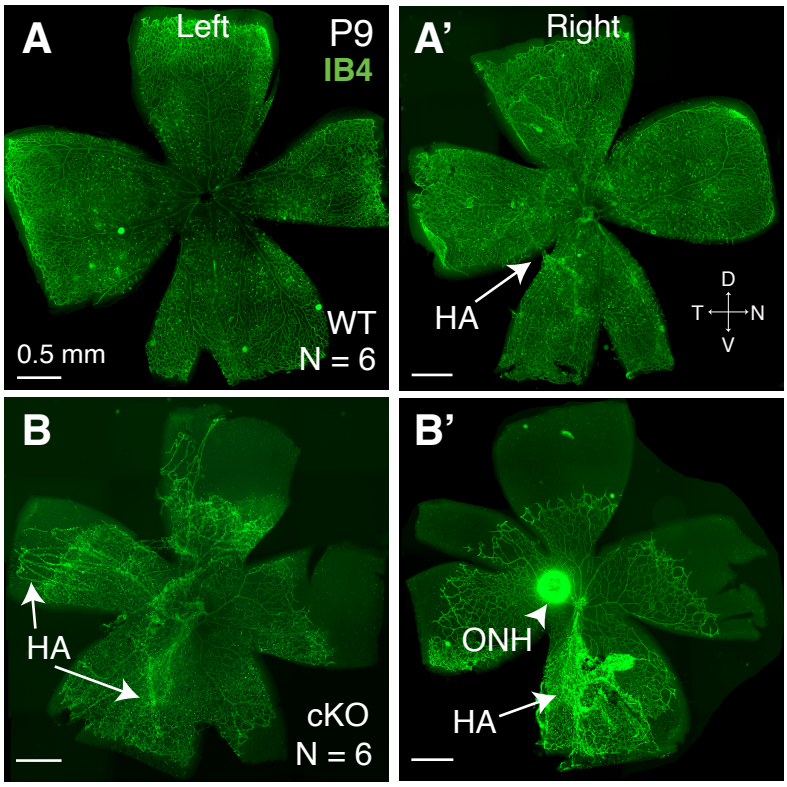

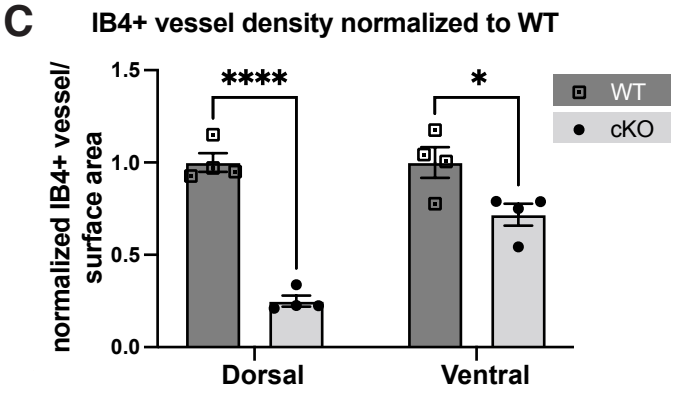

Figure 2. Tbx3 loss results in abnormal blood vessel development.
(A,A') Flat mount P9 retinas from wild-type (WT) and (B,B') conditional Tbx3 knockout retinas (cKO) stained with isolectin GS-B4 (IB4, green) in left and right eyes. Arrows indicate location of hyaloid artery (HA).
(C) Ratio of the vascularized to total retinal surface area in the dorsal and ventral retina normalized to average WT in each litter. Student's two-tailed, unpaired T-test; ****, $p \leq 0.0001$; *, $p=0.01$.

Figure 3

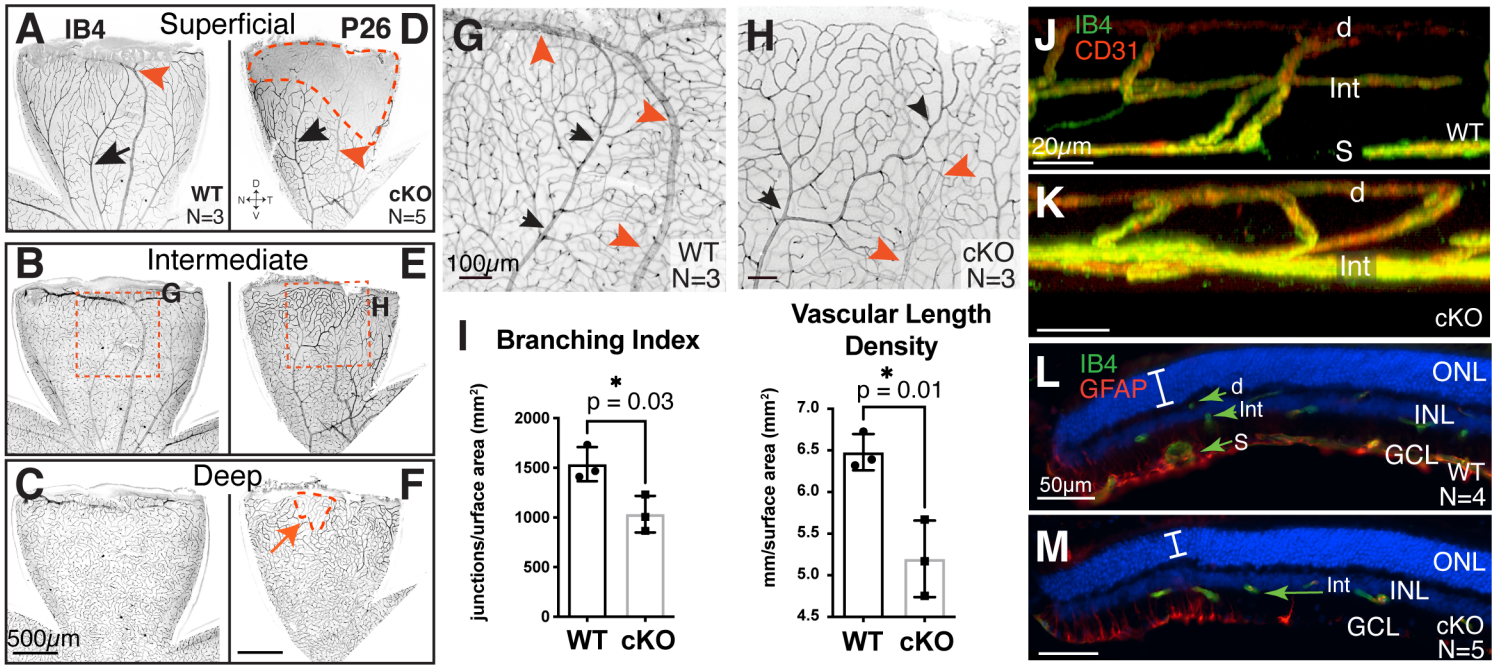

Figure 3. Tbx3 cKO retina fails to form superficial plexus in the adult dorsal retina.
(A-F) Confocal flat mount images of P26 dorsal retinas from wild-type (WT; A,B,C) and conditional knockout (cKO; D,E,F) mice stained with isolectin GS-B4 (IB4). Confocal images are inverted. The superficial (A,D), intermediate (B,E) and deep (C,F) plexus from the same retinal flat mounts are shown.
(G,H) Maximal projection images from a stereomicroscope simultaneously showing all three plexi from the region indicated in B and E. Artery (black arrows) and vein (red arrowheads) in each panel are marked.
(I) Branching index (branch points/retinal surface area) and vascular length density (vessel length/retinal surface area) from maximum projections images (see Fig. S2 for quantitation). Statistical significance was determined using an unpaired, two-tailed T-test; p-values on graph.
(J,K) Still 3D rendered confocal images of retinal plexus in dorsal retina of WT (J) and cKO (K) stained with IB4 (green) and anti-CD31 antibody (red).
(L,M) Transverse cryostat sections of P26 retina stained with IB4 (green) and anti-GFAP antibody (red) to mark endothelial cells and astrocytes, respectively. Superficial (S), intermediate (Int) and deep (d) vascular plexus are marked; outer nuclear layer (ONL), inner nuclear layer (INL), and ganglion cell layer (GCL) can be seen with nuclei marker, DAPI (blue). Note that the anti-GFAP (raised in mouse) antibody lightly stains vascular cells, as these mice were not perfused.

Figure 4

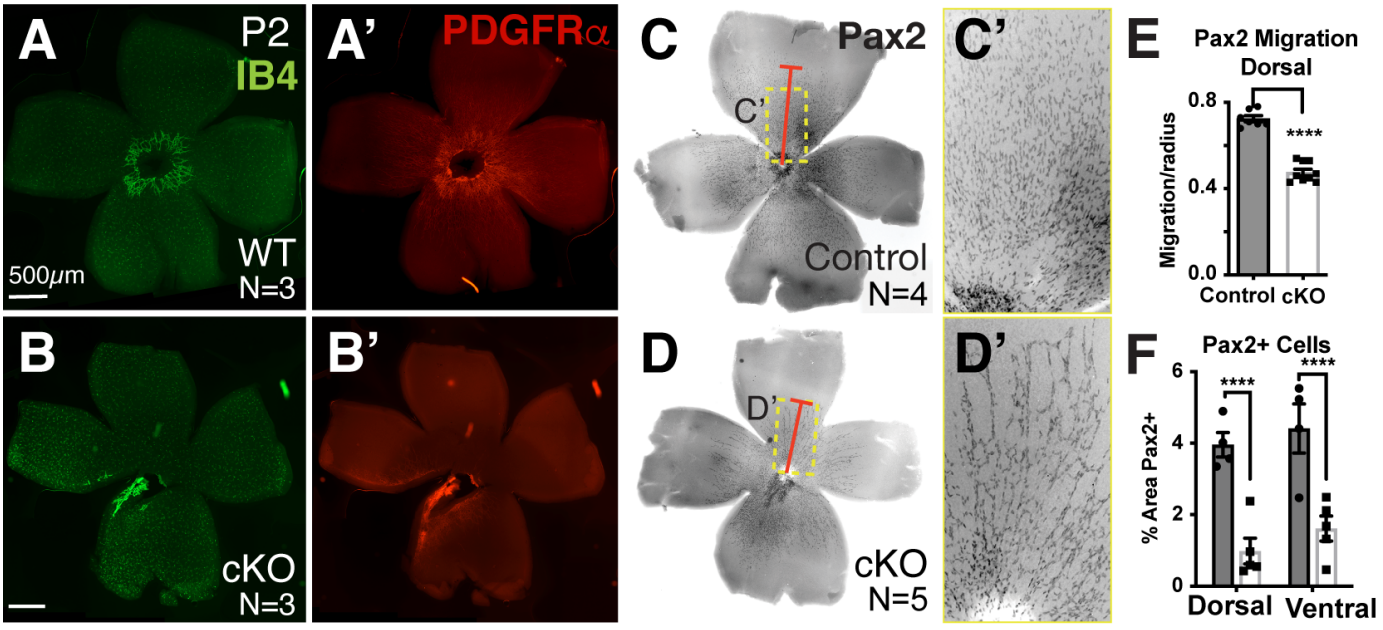

Figure 4. Fewer astrocyte precursors in Tbx3 cKO retinas, starting as early as P2.
(A,B) Endothelial cells are marked with IB4 (green) in WT and Tbx3 cKO flat mounted retinas at P2. (A',B') Same samples immunostained for astrocyte precursors using anti-PDGF receptor alpha (PDGFRα) antibody.
(C,D) Inverse images of flat mount retinas from P2 WT and Tbx3 cKO stained with a second astrocyte precursor marker, anti-Pax2 antibody (black). Red bar marks Pax2-positive cells furthest away from the optic nerve head in each panel. Dashed yellow box indicates images magnified in panels C',D'.
(E) Quantitation of Pax2-positive cells furthest away from optic nerve head in heterozygote (control) and conditional knockout (cKO) retinas. Distance was averaged measure of 10 cells per retina. Unpaired, two-tailed Student's T-test was used to determine significance; ****, $p < 0.0001$.
(F) Graph showing quantitation of the percentage of surface area occupied by dorsal and ventral retinas in control (grey) and cKO (white). Two-way ANOVA test was done to determine statistical significance; ****, $p < 0.0001$; N, number of mice.

Figure 5

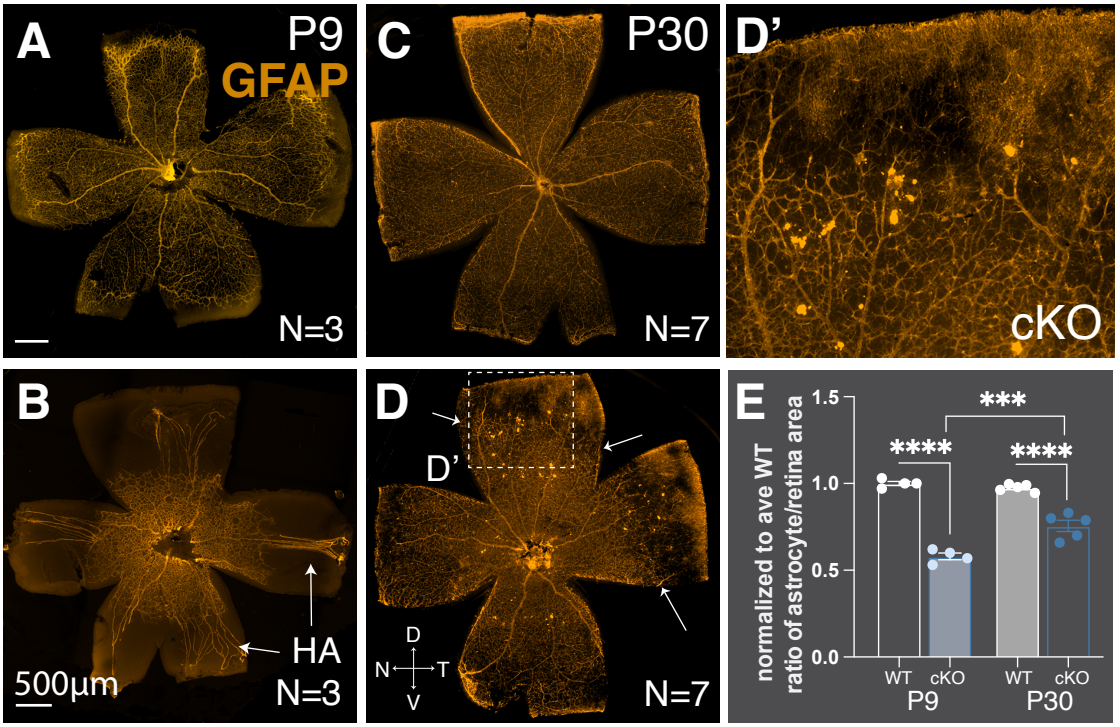

Figure 5. Astrocyte lattice fails to form in dorsal-temporal *Tbx3* cKO retina.
(A,B) Flat mount P9 retinas immunostained with mature astrocyte marker, anti-glial fibrillary acidic protein (GFAP) antibody. Arrows point to the hyaloid artery (HA).
(C,D) Flat mount P30 retinas from WT and cKO mice. Arrows point to the region where the lattice begins thinning in the dorsal and temporal quadrants. Dashed box outlines region magnified in panel D'. Note, artifactual blotches in cKO sample.
(E) Graph quantifying the normalized ratio of astrocyte occupation compared to the retinal surface area for WT and cKO retinas. Dorsal is up in all panels; statistical significance was determined using an ordinary Two-Way ANOVA with multiple comparisons (Tukey); ****, p≤ 0.000.1; ***, p ≤0.001; N, number of mice.

Figure 6

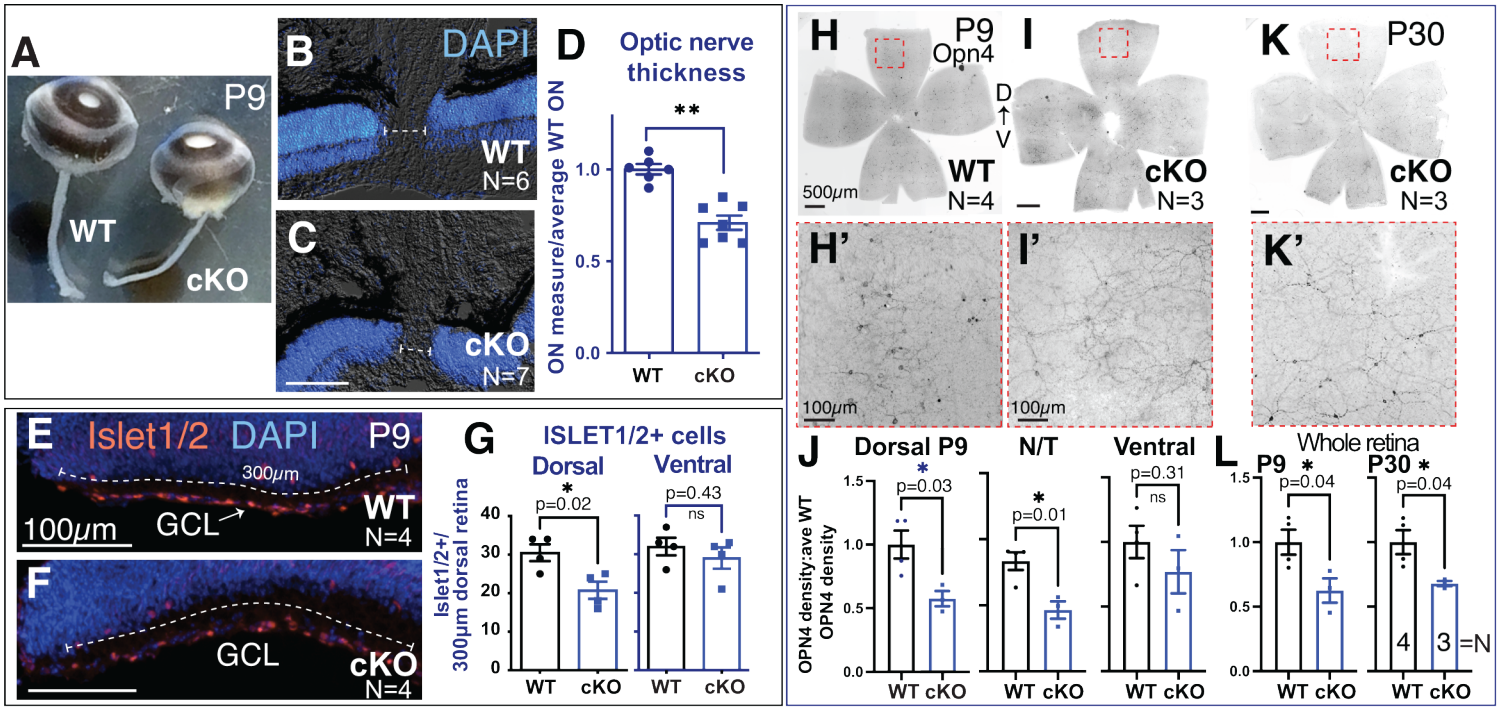

Figure 6. Dorsal specific loss of RGCs with loss of Tbx3.
(A) Snapshot of whole eyes with optic nerves from P9 WT and cKO siblings.
(B,C) Sections of WT and cKO eyes stained with nuclei marker (DAPI) to visualize neural retina. Dashed line indicates optic nerve thickness in each sample.
(D) Graph quantitating the optic nerve thickness in WT and cKO eyes. Statistical significance was measured using an unpaired, two-tailed T-test; **, p = 0.005.
(E-F) Transverse cryostat sections of P9 WT and cKO dorsal tip immunostained with anti-Islet1/2 antibody. The number of Islet1/2-positive cells in the first 300µm of the most dorsal and ventral retina were counted (dashed line). (G) Graphs of the Islet1/2-positive cells in the dorsal and ventral regions.
(H-I') Inverse images of P9 flat mount WT and cKO retinas immunostained with anti-OPN4 antibody marking intrinsically photosensitive ganglion cells (ipRGCs). Dashed box shows area magnified in H' and I'. Density of cells were measured in dorsal, nasal/temporal (N/T) and ventral petals and normalized to WT siblings. (J) Graphs showing quantitation of OPN4-positive cells in each region.
(K) Inverse image of P30 cKO flat mount with magnified area (dashed box) shown in panel K'. (L) Graphs of OPN4-positive cells per whole retina of P9 and P30 samples. An unpaired, two tailed T-test were used to determine statistical significance; p-values on graphs in panels G,J,L; N, number of mice.

References

Aydoğdu, N., Rudat, C., Trowe, M. O., Kaiser, M., Lüdtke, T. H., Taketo, M. M., Christoffels, V. M., Moon, A. and Kispert, A. (2018). TBX2 and TBX3 act downstream of canonical WNT signaling in patterning and differentiation of the mouse ureteric mesenchyme. *Development* **145**,

Behesti, H., Holt, J. K. and Sowden, J. C. (2006). The level of BMP4 signaling is critical for the regulation of distinct T-box gene expression domains and growth along the dorso-ventral axis of the optic cup. *BMC Dev Biol* **6**, 62.

Bosze, B., Suarez-Navarro, J., Soofi, A., Lauderdale, J. D., Dressler, G. R. and Brown, N. L. (2021). Multiple roles for Pax2 in the embryonic mouse eye. *Dev Biol*

Chapman, D. L., Garvey, N., Hancock, S., Alexiou, M., Agulnik, S. I., Gibson-Brown, J. J., Cebra-Thomas, J., Bollag, R. J., Silver, L. M. and Papaioannou, V. E. (1996). Expression of the T-box family genes, Tbx1-Tbx5, during early mouse development. *Dev Dyn* **206**, 379-390.

Chu, Y., Hughes, S. and Chan-Ling, T. (2001). Differentiation and migration of astrocyte precursor cells and astrocytes in human fetal retina: relevance to optic nerve coloboma. *FASEB J* **15**, 2013-2015.

Collin, R. W., Nikopoulos, K., Dona, M., Gilissen, C., Hoischen, A., Boonstra, F. N., Poulter, J. A., Kondo, H., Berger, W., Toomes, C. et al. (2013). ZNF408 is mutated in familial exudative vitreoretinopathy and is crucial for the development of zebrafish retinal vasculature. *Proc Natl Acad Sci U S A* **110**, 9856-9861.

Daneman, R., Agalliu, D., Zhou, L., Kuhnert, F., Kuo, C. J. and Barres, B. A. (2009). Wnt/beta-catenin signaling is required for CNS, but not non-CNS, angiogenesis. *Proc Natl Acad Sci U S A* **106**, 641-646.

Davenport, T. G., Jerome-Majewska, L. A. and Papaioannou, V. E. (2003). Mammary gland, limb and yolk sac defects in mice lacking Tbx3, the gene mutated in human ulnar mammary syndrome. *Development* **130**, 2263-2273.

Dhingra, S., Shears, D. J., Blake, V., Stewart, H. and Patel, C. K. (2006). Advanced bilateral persistent fetal vasculature associated with a novel mutation in the Norrie gene. *Br J Ophthalmol* **90**, 1324-1325.

Dorrell, M. I., Aguilar, E. and Friedlander, M. (2002). Retinal vascular development is mediated by endothelial filopodia, a preexisting astrocytic template and specific R-cadherin adhesion. *Invest Ophthalmol Vis Sci* **43**, 3500-3510.

Edwards, M. M., McLeod, D. S., Li, R., Grebe, R., Bhutto, I., Mu, X. and Lutty, G. A. (2012). The deletion of Math5 disrupts retinal blood vessel and glial development in mice. *Exp Eye Res* **96**, 147-156.

Emechebe, U., Kumar P, P., Rozenberg, J. M., Moore, B., Firment, A., Mirshahi, T. and Moon, A. M. (2016). T-box3 is a ciliary protein and regulates stability of the Gli3 transcription factor to control digit number. *Elife* **5**,

Frank, D. U., Carter, K. L., Thomas, K. R., Burr, R. M., Bakker, M. L., Coetzee, W. A., Tristani-Firouzi, M., Bamshad, M. J., Christoffels, V. M. and Moon, A. M. (2012). Lethal arrhythmias in Tbx3-deficient mice reveal extreme dosage sensitivity of cardiac conduction system function and homeostasis. *Proc Natl Acad Sci U S A* **109**, 154-163.

Frank, D. U., Emechebe, U., Thomas, K. R. and Moon, A. M. (2013). Mouse TBX3 mutants suggest novel molecular mechanisms for Ulnar-mammary syndrome. *PLoS One* **8**, e67841.

Fruttiger, M. (2007). Development of the retinal vasculature. *Angiogenesis* **10**, 77-88.

Fruttiger, M., Calver, A. R., Krüger, W. H., Mudhar, H. S., Michalovich, D., Takakura, N., Nishikawa, S. and Richardson, W. D. (1996). PDGF mediates a neuron-astrocyte interaction in the developing retina. *Neuron* **17**, 1117-1131.

Jiang, B., Bezhadian, M. A. and Caldwell, R. B. (1995). Astrocytes modulate retinal vasculogenesis: effects on endothelial cell differentiation. *Glia* **15**, 1-10.

Jiang, B., Liou, G. I., Behzadian, M. A. and Caldwell, R. B. (1994). Astrocytes modulate retinal vasculogenesis: effects on fibronectin expression. *J Cell Sci* **107**, 2499-2508.

Junge, H. J., Yang, S., Burton, J. B., Paes, K., Shu, X., French, D. M., Costa, M., Rice, D. S. and Ye, W. (2009). TSPAN12 regulates retinal vascular development by promoting Norrin- but not Wnt-induced FZD4/beta-catenin signaling. *Cell* **139**, 299-311.

Kaiser, M., Wojahn, I., Rudat, C., Lüdtke, T. H., Christoffels, V. M., Moon, A., Kispert, A. and Trowe, M. O. (2021). Regulation of otocyst patterning by Tbx2 and Tbx3 is required for inner ear morphogenesis in the mouse. *Development* dev.195651.

Kumar P, P., Franklin, S., Emechebe, U., Hu, H., Moore, B., Lehman, C., Yandell, M. and Moon, A. M. (2014). TBX3 regulates splicing in vivo: a novel molecular mechanism for Ulnar-mammary syndrome. *PLoS Genet* **10**, e1004247.

Li, J. K., Li, Y., Zhang, X., Chen, C. L., Rao, Y. Q., Fei, P., Zhang, Q., Zhao, P. and Li, J. (2018). Spectrum of Variants in 389 Chinese Probands With Familial Exudative Vitreoretinopathy. *Invest Ophthalmol Vis Sci* **59**, 5368-5381.

Lüdtke, T. H., Rudat, C., Wojahn, I., Weiss, A. C., Kleppa, M. J., Kurz, J., Farin, H. F., Moon, A., Christoffels, V. M. and Kispert, A. (2016). Tbx2 and Tbx3 Act Downstream of Shh to Maintain Canonical Wnt Signaling during Branching Morphogenesis of the Murine Lung. *Dev Cell* **39**, 239-253.

Luhmann, U. F., Lin, J., Acar, N., Lammel, S., Feil, S., Grimm, C., Seeliger, M. W., Hammes, H. P. and Berger, W. (2005). Role of the Norrie disease pseudoglioma gene in sprouting angiogenesis during development of the retinal vasculature. *Invest Ophthalmol Vis Sci* **46**, 3372-3382.

Lyu, P., Hoang, T., Santiago, C. P., Thomas, E. D., Timms, A. E., Appel, H., Gimmen, M., Le, N., Jiang, L., Kim, D. W. et al. (2021). Gene regulatory networks controlling temporal patterning, neurogenesis, and cell-fate specification in mammalian retina. *Cell Rep* **37**, 109994.

Mao, C. A., Li, H., Zhang, Z., Kiyama, T., Panda, S., Hattar, S., Ribelayga, C. P., Mills, S. L. and Wang, S. W. (2014). T-box transcription regulator Tbr2 is essential for the formation and maintenance of Opn4/melanopsin-expressing intrinsically photosensitive retinal ganglion cells. *J Neurosci* **34**, 13083-13095.

Martinez-De Luna, R. I., Ku, R. Y., Lyou, Y. and Zuber, M. E. (2013). Maturin is a novel protein required for differentiation during primary neurogenesis. *Dev Biol* **384**, 26-40.

Mi, H. and Barres, B. A. (1999). Purification and characterization of astrocyte precursor cells in the developing rat optic nerve. *J Neurosci* **19**, 1049-1061.

Mi, H., Haeberle, H. and Barres, B. A. (2001). Induction of astrocyte differentiation by endothelial cells. *J Neurosci* **21**, 1538-1547.

Miyawaki, T., Uemura, A., Dezawa, M., Yu, R. T., Ide, C., Nishikawa, S., Honda, Y., Tanabe, Y. and Tanabe, T. (2004). Tlx, an orphan nuclear receptor, regulates cell numbers and astrocyte development in the developing retina. *J Neurosci* **24**, 8124-8134.

Motahari, Z., Martinez-De Luna, R. I., Viczian, A. S. and Zuber, M. E. (2016). Tbx3 represses bmp4 expression and with Pax6 is required and sufficient for retina formation. *Development* **143**, 3560-3572.

Nguyen, M. T., Vemaraju, S., Nayak, G., Odaka, Y., Buhr, E. D., Alonzo, N., Tran, U., Batie, M., Upton, B. A., Darvas, M. et al. (2019). An opsin 5-dopamine pathway mediates light-dependent vascular development in the eye. *Nat Cell Biol* **21**, 420-429.

O'Sullivan, M. L., Puñal, V. M., Kerstein, P. C., Brzezinski, J. A., Glaser, T., Wright, K. M. and Kay, J. N. (2017). Astrocytes follow ganglion cell axons to establish an angiogenic template during retinal development. *Glia* **65**, 1697-1716.

Paisley, C. E. and Kay, J. N. (2021). Seeing stars: Development and function of retinal astrocytes. *Dev Biol* **478**, 144-154.

Park, E. J., Sun, X., Nichol, P., Saijoh, Y., Martin, J. F. and Moon, A. M. (2008). System for tamoxifen-inducible expression of cre-recombinase from the Foxa2 locus in mice. *Dev Dyn* **237**, 447-453.

Payabvash, S., Anderson, J. S. and Nascene, D. R. (2015). Bilateral persistent fetal vasculature due to a mutation in the Norrie disease protein gene. *Neuroradiol J* **28**, 623-627.

Pendergast, S. D., Trese, M. T., Liu, X. and Shastry, B. S. (1998). Study of the Norrie disease gene in 2 patients with bilateral persistent hyperplastic primary vitreous. *Arch Ophthalmol* **116**, 381-382.

Perelli, R. M., O'Sullivan, M. L., Zarnick, S. and Kay, J. N. (2021). Environmental oxygen regulates astrocyte proliferation to guide angiogenesis during retinal development. *Development* **148**, dev199418.

Quarta, C., Fisette, A., Xu, Y., Colldén, G., Legutko, B., Tseng, Y.-T., Reim, A., Wierer, M., De Rosa, M. C., Klaus, V. R., R Thaker, V V Graf, E et al. (2019). Functional identity of hypothalamic melanocortin neurons depends on Tbx3. *Nature Metabolism* **1**, 222.

Rao, F. Q., Cai, X. B., Cheng, F. F., Cheng, W., Fang, X. L., Li, N., Huang, X. F., Li, L. H. and Jin, Z. B. (2017). Mutations in LRP5,FZD4, TSPAN12, NDP, ZNF408, or KIF11 Genes Account for 38.7% of Chinese Patients With Familial Exudative Vitreoretinopathy. *Invest Ophthalmol Vis Sci* **58**, 2623-2629.

Rao, S., Chun, C., Fan, J., Kofron, J. M., Yang, M. B., Hegde, R. S., Ferrara, N., Copenhagen, D. R. and Lang, R. A. (2013). A direct and melanopsin-dependent fetal light response regulates mouse eye development. *Nature*

Robitaille, J. M., Wallace, K., Zheng, B., Beis, M. J., Samuels, M., Hoskin-Mott, A. and Guernsey, D. L. (2009). Phenotypic overlap of familial exudative vitreoretinopathy (FEVR) with persistent fetal vasculature (PFV) caused by FZD4 mutations in two distinct pedigrees. *Ophthalmic Genet* **30**, 23-30.

Sato, S., Inoue, T., Terada, K., Matsuo, I., Aizawa, S., Tano, Y., Fujikado, T. and Furukawa, T. (2007). Dkk3-Cre BAC transgenic mouse line: a tool for highly efficient gene deletion in retinal progenitor cells. *Genesis* **45**, 502-507.

Selvam, S., Kumar, T. and Fruttiger, M. (2018). Retinal vasculature development in health and disease. *Prog Retin Eye Res* **63**, 1-19.

Soukkarieh, C., Agius, E., Soula, C. and Cochard, P. (2007). Pax2 regulates neuronal-glial cell fate choice in the embryonic optic nerve. *Dev Biol* **303**, 800-813.

Sowden, J. C., Holt, J. K., Meins, M., Smith, H. K. and Bhattacharya, S. S. (2001). Expression of Drosophila omb-related T-box genes in the developing human and mouse neural retina. *Invest Ophthalmol Vis Sci* **42**, 3095-3102.

Stalmans, I., Ng, Y. S., Rohan, R., Fruttiger, M., Bouché, A., Yuce, A., Fujisawa, H., Hermans, B., Shani, M., Jansen, S. et al. (2002). Arteriolar and venular patterning in retinas of mice selectively expressing VEGF isoforms. *J Clin Invest* **109**, 327-336.

Stone, J., Itin, A., Alon, T., Pe'er, J., Gnessin, H., Chan-Ling, T. and Keshet, E. (1995). Development of retinal vasculature is mediated by hypoxia-induced vascular endothelial growth factor (VEGF) expression by neuroglia. *J Neurosci* **15**, 4738-4747.

Sun, Y. and Smith, L. E. H. (2018). Retinal Vasculature in Development and Diseases. *Annu Rev Vis Sci* **4**, 101-122.

Takabatake, Y., Takabatake, T. and Takeshima, K. (2000). Conserved and divergent expression of T-box genes Tbx2-Tbx5 in Xenopus. *Mech Dev* **91**, 433-437.

Tang, M., Sun, L., Hu, A., Yuan, M., Yang, Y., Peng, X. and Ding, X. (2017). Mutation Spectrum of the LRP5, NDP, and TSPAN12 Genes in Chinese Patients With Familial Exudative Vitreoretinopathy. *Invest Ophthalmol Vis Sci* **58**, 5949-5957.

Tao, C. and Zhang, X. (2014). Development of astrocytes in the vertebrate eye. *Dev Dyn* **243**, 1501-1510.

Tauqeer, Z. and Yonekawa, Y. (2018). Familial Exudative Vitreoretinopathy: Pathophysiology, Diagnosis, and Management. *Asia Pac J Ophthalmol (Phila)* **7**, 176-182.

Uemura, A., Kusuhara, S., Wiegand, S. J., Yu, R. T. and Nishikawa, S. (2006). Tlx acts as a proangiogenic switch by regulating extracellular assembly of fibronectin matrices in retinal astrocytes. *J Clin Invest* **116**, 369-377.

Usui, Y., Westenskow, P. D., Kurihara, T., Aguilar, E., Sakimoto, S., Paris, L. P., Wittgrove, C., Feitelberg, D., Friedlander, M. S., Moreno, S. K. et al. (2015). Neurovascular crosstalk between interneurons and capillaries is required for vision. *J Clin Invest* **125**, 2335-2346.

Viczian, A. S., Vignali, R., Zuber, M. E., Barsacchi, G. and Harris, W. A. (2003). XOtx5b and XOtx2 regulate photoreceptor and bipolar fates in the Xenopus retina. *Development* **130**, 1281-1294.

Wang, Y., Smallwood, P. M., Williams, J. and Nathans, J. (2020). A mouse model for Kinesin Family Member 11 (Kif11)-associated familial exudative vitreoretinopathy. *Hum Mol Genet*

Weidgang, C. E., Russell, R., Tata, P. R., Kühl, S. J., Illing, A., Müller, M., Lin, Q., Brunner, C., Boeckers, T. M., Bauer, K. et al. (2013). TBX3 Directs Cell-Fate Decision toward Mesendoderm. *Stem Cell Reports* **1**, 248-265.

Weiner, G. A., Shah, S. H., Angelopoulos, C. M., Bartakova, A. B., Pulido, R. S., Murphy, A., Nudleman, E., Daneman, R. and Goldberg, J. L. (2019). Cholinergic neural activity directs retinal layer-specific angiogenesis and blood retinal barrier formation. *Nat Commun* **10**, 2477.

Wong, K., Peng, Y., Kung, H. F. and He, M. L. (2002). Retina dorsal/ventral patterning by Xenopus TBX3. *Biochem Biophys Res Commun* **290**, 737-742.

Wong, K. A., Trembley, M., Abd Wahab, S. and Viczian, A. S. (2015). Efficient retina formation requires suppression of both Activin and BMP signaling pathways in pluripotent cells. *Biol Open* **4**, 573-583.

Wu, W. C., Drenser, K., Trese, M., Capone, A. and Dailey, W. (2007). Retinal phenotype-genotype correlation of pediatric patients expressing mutations in the Norrie disease gene. *Arch Ophthalmol* **125**, 225-230.

Ye, X., Wang, Y., Cahill, H., Yu, M., Badea, T. C., Smallwood, P. M., Peachey, N. S. and Nathans, J. (2009). Norrin, frizzled-4, and Lrp5 signaling in endothelial cells controls a genetic program for retinal vascularization. *Cell* **139**, 285-298.

Ye, X., Wang, Y. and Nathans, J. (2010). The Norrin/Frizzled4 signaling pathway in retinal vascular development and disease. *Trends Mol Med* **16**, 417-425.

Zhang, Y. and Stone, J. (1997). Role of astrocytes in the control of developing retinal vessels. *Invest Ophthalmol Vis Sci* **38**, 1653-1666.

Zimmerli, D., Borrelli, C., Jauregi-Miguel, A., Söderholm, S., Brütsch, S., Doumpas, N., Reichmuth, J., Murphy-Seiler, F., Aguet, M., Basler, K. et al. (2020). TBX3 acts as tissue-specific component of the Wnt/β-catenin transcriptional complex. *Elife* **9**,

Zuber, M. E., Gestri, G., Viczian, A. S., Barsacchi, G. and Harris, W. A. (2003). Specification of the vertebrate eye by a network of eye field transcription factors. *Development* **130**, 5155-5167.